Estimation of the Mechanical Property of CNT Ropes Using Atomistic-Continuum Mechanics and the Equivalent Methods

C.J. Huang[1], T.Y. Hung[1], K.N. Chiang[2]

Abstract: The development in the field of nanotechnology has prompted numerous researchers to develop various simulation methods for determining the material properties of nanoscale structures. However, these methods are restricted by the speed limitation of the central processing unit (CPU), which cannot estimate larger-scale nanoscale models within an acceptable time. Thus, decreasing the CPU processing time and retaining the estimation accuracy of physical properties of nanoscale structures have become critical issues. Accordingly, this study aims to decrease the CPU processing time and complexity of large nanoscale models by utilizing, atomistic-continuum mechanics (ACM) to build an equivalent model of carbon nanotubes (CNTs). The results of tensile and modal analyses agree with previous experimental results indicating that the ACM model can accurately describe mechanical properties. This study also adopted three definitions of cross-sectional area to explore whether the structure properties of CNT ropes depends on the definitions of cross-sectional area. Results indicate that the Young's modulus distribution based on the circumcircle assumptions agrees well with most of the experimental results. Hence, most experimental methods adopted the circumcircle to obtain the Young's modulus of the CNT ropes. The circumcircle assumption involves the distribution of the tubes and the gap between each tube. The ratio between the gap and tube areas becomes a stable value when the diameter of the CNT ropes is increased. Therefore, a larger diameter of CNT ropes that represents the Young's modulus becomes a stable value, as mentioned in literature. This study also investigated the equivalent solid, shell, and beam models to generate similar mechanical behaviors with the ACM model. The similar mechanical behavior of the equivalent model includes the model under tensile, torsion, or shear external loading. These equivalent models can significantly reduce the required total element number and CPU processing time to investigate a larger nanoscale structure.

---

[1] Research Engineer, TSMC/NTHU, Hsinchu, Taiwan, R. O. C.

[2] Corresponding Author, NTHU, Hsinchu, Taiwan, R. O. C.; E-mail:knchiang@pme.nthu.edu.tw; Tel: +886-3-571-42925; Fax: +886-3-574-5377.

Keywords: atomistic-continuum mechanics method, finite-element method, equivalent method, multi-scale structures, Young's modulus, carbon nanotubes.

1   Introduction

In the past three decades, nanotechnology has been a pioneer in the discovery of innovative material properties and applications. Most studies aimed at identifying the particular properties of nanoscale structures. Many simulation methodologies have been proposed to obtain the material properties of nanoscale structures, such as Quantum Mechanics, Molecular Dynamics (MD), or Monte Carlo (MC), which are suitable for different situations. Computational ability for atomistic simulations that are utilized in the nanoscale material behavior with good performance is continuously increasing, but the computational ability of these numerical simulation methods cannot simulate a nanoscale structure that contains more than a few billion atoms. The atomistic-continuum mechanics (ACM) method has recently been developed to overcome the limitation of the computational ability and to calculate the nanostructure with higher efficiency than that of the other aforementioned methods. The ACM is built on the concepts of atomic mechanics, continuum mechanics, finite element method (FEM), and the equilibrium method. ACM has also been adopted to investigate a larger nanoscale structure for years, and it is a reliable and acceptable technique used for numerical simulations and experiment validation.

The extraordinary material properties of CNTs were first discovered in 1991 by Iijima (1991) in the NEC laboratory in Japan. Carbon nanotubes (CNTs) contain ultra-high Young's modulus, thermal conductivity, and high aspect ratio. These characteristics make CNTs to be the most exciting new materials to have been exhibited in the past three decades. Many studies on the field of CNT modeling have been conducted in the last decade. These studies can be generalized into two main simulation methods, namely, atomistic-based and continuum-based models. Tserpesa and Papanikos (2009) presented CNT-based super-nanotubes, super-graphene, and super-square, all of which were modeled using the equivalent beam concept via MD simulations. Chang (2007) used molecular mechanics simulations to investigate the mechanical response of single-walled carbon nanotubes (SWNTs) under torsion. Liu, Jiang, Huang, Qu, Yu, and Hwang (2005) developed an atomic-scale FEM (AFEM) with the same formal structure as the continuum FEM, in which the interactions within similar CNTs were characterized using the Brenner potential with the AFEM element. Jalalahmadi and Naghdabadi (2006) demonstrated the applicability of the FEM model and the new wall thickness, as well as the influence of tube wall thickness, diameter, and chirality on the Young's modulus of SWNTs. Ruoff, Qian, and Liu (2003) discussed the elastic properties of CNTs in terms of deformability (e.g., buckling, twisting, flattening, and inelastic behav-

ior). Rossi and Meo (2009) provided an SWNT-FEM model by using nonlinear and torsional spring elements to evaluate the mechanical properties of the Young's modulus. Jeng, Tsai, Huang, and Chang (2009) investigated a series of Molecular Statics and MD simulations to investigate the mechanical properties of SWCNTs under a uniaxial tensile strain.

The spring network models were widely utilized in FEM based nanostructure studies in the previous study [Gusev (2004); Chung, Hosson, and Giessen (2002); Chiang, Chou, Wu, and Yuan (2006)] analyzed an atomic-level single-lattice method by using a closed-form equation to predict the elastic characteristics of bulk metals. Many nanoscale studies [Iijima (1991); Sun, and Chen (2009); Salvetat, Briggs, Bonard, Bacsa, Kulik, Stöckli, Burnham, and Forró (1999); Lawrence, Berhan, and Nadarajah (2009); Poncharal, Wang, Ugarte, and de Heer(1999)] aimed at identifying and understanding the innovative properties of CNTs. Wu Chou, Han, and Chiang (2009) proposed the ACM method to discuss tensile and vibration analyses. Chiang, Chou, Wu, Huang, and Yew (2008) adopted the ACM and FEM to construct an equivalent-continuum model to investigate the mechanical properties of CNT. The results showed that the Young's modulus wouldn't change obviously with the variation of tube radius and length, and the average of Young's modulus is about 1,050 GPa with agreed with the most experimental and analytical results.

The ACM method established in the FEM with equivalent spring elements are used to analysis the Young's modulus using the tensile and the modal behavior in the nanoscale (atomic scale) structure. The ACM atomic model is not only suitable for the axial tensile loading condition, but also for modal analysis. The results from both tensile and modal analyses agree well with the experimental results described in literature. Moreover, this novel simulation method for investigating nanoscale materials is not limited to specific materials; it can also be applied to any hetero-material when the inter-atomic potential and the atomic structure of the material are known. Several studies used the ACM method to validate its acceptability and reliability. The ACM method depends on two factors. First, the potential function should be based on known properties. If one is interested in the properties of a new type of molecule, an appropriate force field might not be available for that type of molecules. Second, the electronic properties of molecule prediction are not applicable because ACM models are assembled by groups of springs.

Although the single CNT yields good mechanical, thermal, and electrical performances, it still has limitations in terms of the Young's modulus and the diameter of the CNT ropes. That might attribute to the different experimental method adopting the different cross-sectional area types in the CNT ropes. Sun and Chen (2009) designed an experiment to test the tensile strength of CNT-reinforced copper composites with different diameters, through which they found a parabolic re-

lationship between the CNT diameter and the resultant tensile strength. Salvetat, Briggs, Bonard, Bacsa, Kulik, Stöckli, Burnham, and Forró, (1999) used an atomic force microscopy (AFM) and a special substrate to determine the elastic and shear moduli of SWNT ropes, which were measured to be in the order of 1 TPa and 1 GPa, respectively. Lawrence, Berhan, and Nadarajah (2009) proposed a three-point bending test process by using AFM and transmission electron microscopy (TEM) to suspend individual nanofibers and measure their deflection accurately. Cheng, Hsu, and Chen, (2009) used MD simulation to investigate atomistic defects in SWCNTs on their nanomechanical properties.

Poncharal, Wang, Ugarte, and de Heer (1999) used resonant information on individual nanotubes to investigate the tendencies in elastic modulus with different nanotube diameter. Chen, Zhang, Dikin, Ding, Ruoff, Pan, and Nakayama (2003) characterized the mechanical properties of a nanocoil established on a nonlinear relationship between the spring constant of the nanocoil and the shear modulus, in which the contributions of all components of the restoring force were involved. Yu, Files, Arepalli, and Ruoff (2000) investigated the mechanical response of 15 SWNT ropes under a tensile load, in which the values of the Young's modulus ranged from 320 GPa to 1,470 GPa, with the mean value of 1,002 GPa. Krishnan, Dujardin, Ebbesen, Yianilos, and Treacy (1998) estimated the stiffness of SWNTs by observing their free-standing room temperature vibrations via TEM. Fan, Liu, and Hwu (2009) discussed the relationship between the mechanical properties and the nanotube size of CNTs, and found that mechanical properties are dependent on the diameter of the CNTs. Kis, Cs?nyi, Salvetat, Lee, Couteau, Kulik, Benoit, Brugger, and Forr? (2004) proposed that the bending modulus of CNT ropes is dependent on the tube diameter. ?vila and Lacerda (2008) proved that CNT configuration influences stiffness. By varying the radius and the curvature, the Young's modulus increased from 0.95 TPa to 5.5 TPa, and the Poisson's ratio ranged from 0.15 to 0.29. The numerical simulations were in good agreement with those presented in literature. This study investigates three typical cross-sectional area definitions to explore whether the Young's modulus of CNT ropes depends on the cross-sectional area definition. Individual CNTs showed an elastic constant that matches with the constant value acquired in most literature results. However, the mechanical strength of CNT ropes exhibited highly dependent on the cross-sectional area definitions.

To consider the mechanical behavior of the atomic groups, the clustered atomistic investigation should be based on the classic macro-micro numerical analysis procedure. The macro-micro technique, also known as the equivalent method or the global-local, was first established in the 1970s. Mote (1971) proposed a global-local FEM analysis concept and defined specific parts of the analysis domain as the local areas, which where modeled using the fine mesh or high-order finite el-

ement. The local areas were often defined as the mechanically interested region or the areas with high stress concentration. Alternatively, the other domains were defined as global areas, which were established using a coarse mesh or a low-order element. Mote (1971) also used a global-local linking stiffness matrix to combine the two stiffness matrices of the global and local areas. The computations of the local and global areas were thus accomplished simultaneously. Therefore, this FEM technique could obtain mechanical information on the local area with limited calculating capability. Wang and Corssman (1977) applied the concept of the effective modulus to investigate the extensional response of multi-layered structures.

Voleti, Chandra, and Miller (1996) proposed the micro-macro FEM technique and defined the stiffness of the micro model, after which they used this stiffness as a material property in the macro model. The result of the macro model was extracted and regarded as the loading condition of the micro model. Hence, although the macro model used the coarse mesh, the mechanical characteristics of the micro model with fine mesh were suitably considered in the macro model. The equivalent method is the major technique used for overcoming CPU limitations. The equivalent method involves searching for the equivalent element that can demonstrate the material mechanical behavior based on the ACM model. This multi-scale model can reduce computational modeling and simulation time to obtain the material properties and maintain the level of accuracy.

2 Methods

2.1 Introduction of ACM

The ACM is a novel atomistic level numerical methodology based on the elastic finite element theory. The ACM method transfers an originally discrete atomic structure into an equilibrium continuum model by using atomistic-continuum transfer elements. All inter-atomic forces described using the empirical potential function can be transferred into the atomic force with springs to construct the atomic structure. The spring network models are also utilized in FEM-based nanostructure studies.

The movement of an atom from its equilibrium position involves attractive and repulsive behaviors as shown in Fig.1. If an atom is pulled to increase its distance from another atom, the spring yields an attractive force on the atom and attempt to attract it back to its equilibrium position. If the atoms are pushed closer to each other, the spring produces a repulsive force on the atom and restores the single atom to its equilibrium position. The relationship between the interaction force and the elongation of diatom (r) is derived from the differentiation of the potential function

(E_{bond}) with regards to the position of the atom, i.e.,

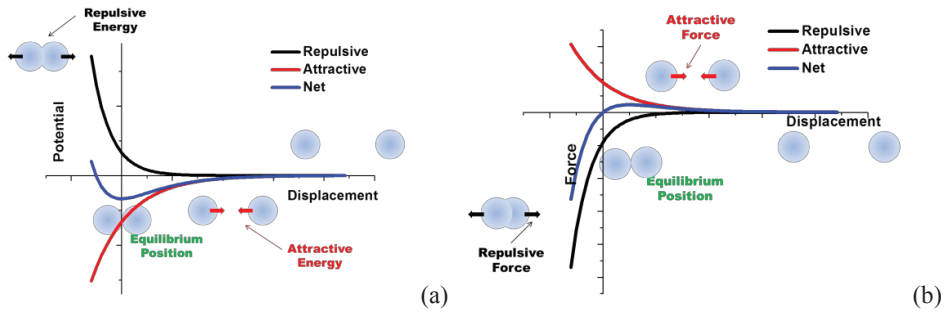$$F_{bonds} = \frac{\partial E_{bond}}{\partial r} \tag{1}$$

Figure 1: The relationship between (a) potential and bond length. (b) interaction force and bond stretching.

The mean positions of the atoms of the elements can be regarded as the positions that can obtain the minimum total energy. To move one atom aside from its equilibrium position requires stretching/compressing or attractive/repulsive behavior. The minimization of the total potential energy is considered due to the ACM. Therefore, this section utilizes the principle of minimum potential energy. For example, Fig. 2 shows the face centered cubic (FCC) lattice structure transfer from the discrete atomic structure into an equilibrium spring element. All inter-atomic forces described using the empirical potential function can be transferred into the atomic force with springs to construct the lattice structure.
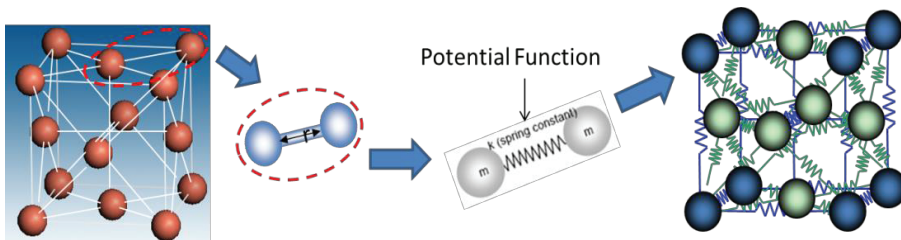

Figure 2: ACM method in the FCC lattice.

Although researchers have developed equivalent methods to determine chemical bonds, the accurate cross-sectional area of the equivalent continuum element, such

as the truss, beam, or solid element, should be defined. This research utilized ACM to estimate the mechanical properties of an atomic structure by applying an appropriate potential energy. Therefore, equivalent spring elements were utilized this study. Spring elements have two characteristics that are distinct from those of prior elements. Spring elements cannot be bent, and the cross-sectional area cannot be defined. According to these two characteristics, spring elements can represent a more realistic equivalent model because the chemical bond can neither be bent nor be defined by a cross-sectional area. Two assumptions exist in the ACM model: (1) the structure is without any defect, and (2) the structure only experiences small deformations. The various diatom distances should be less than the material properties obtained from the relationship between the displacement and the diatom force.

This study utilized the ACM model to investigate an atomic-scale/nanoscale model for tensile and modal investigations to estimate the mechanical properties of an atomic-level structure by using a proper potential energy. The numerical model tested using ANSYS® obtained the reaction forces and natural frequencies of the nanostructures that assisted in the derivation of the mechanical properties of the nanostructures. Overall, the distinct feature of the ACM method lies in its usage of the same model for tensile and modal analyses. In the tensile analysis, the Young's modulus could be defined as the ratio between the normal stress σ and the normal strain ε based on the Hooke's law as shown in Eq. (2)

$$E = \sigma/\varepsilon \qquad (2)$$

Furthermore, the normal stress σ can be expressed as the force per unit area, stress is a measure of the internal forces acting within a deformable test vehicle. Quantitatively, it is a measure of the average force per unit area of a surface within the test vehicle. The normal strain ε can be defined as the ratio of total deformation to the initial dimension of the test vehicle in which the forces are being applied. Hence, the Young's modulus E can be defined as the ratio of the normal stress σ to the normal strain ε under a uniaxial tension condition as Eq. (3) and Fig. 3

$$E = \frac{F_{total}/A}{\Delta l/l} \qquad (3)$$

where F_{total} is the total reaction force, ε represents the applied tensile strain loading, which is the elongation per length, A represents the equivalent area in the ACM model, l is the total length of the structure, and Δl denotes the small prescribed extension length.

Tensile testing is the most common strategy to obtain the Young's modulus of a structure. As nano-scale structures might be too small to test, the alternative strategy applies modal testing to overcome this limitation. The Young's modulus can be

Boundary Condition and Undeform Diagram

Cross-sectional Area   Fixed side   Tensile loading

A

l

Total length

Free Body Diagram and Deform Diagram

F_{total}

Total reaction force $\varDelta l$
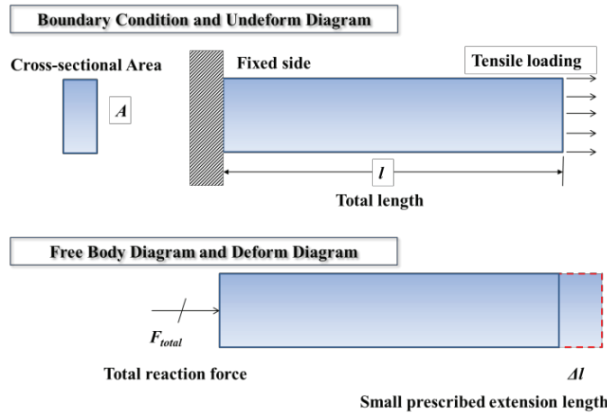
Small prescribed extension length

Figure 3: Tensile analysis in the beam structure

derived based on the resonant frequency by using the Euler-Bernoulli beam theory [Rao, S. S. (2005)]. Euler-Bernoulli beam theory is a simplification of the linear theory of elasticity which provides a means of calculating the load-carrying and deflection characteristics of beams. This theory covers the case for small deflections of a beam which is subjected to lateral loads only. It is thus a special case of Timoshenko beam theory which accounts for shear deformation and is applicable for thick beams. In the modal analysis, consider the free-body diagram of an element of a beam shown in Fig. 4.

Z

$f(x,t)$

X

x dx

L

$f(x,t)$

$\rho A(x)dx\dfrac{\partial^2 w(x,t)}{\partial t^2}$

$M(x,t)$ $M(x,t)+dM(x,t)$
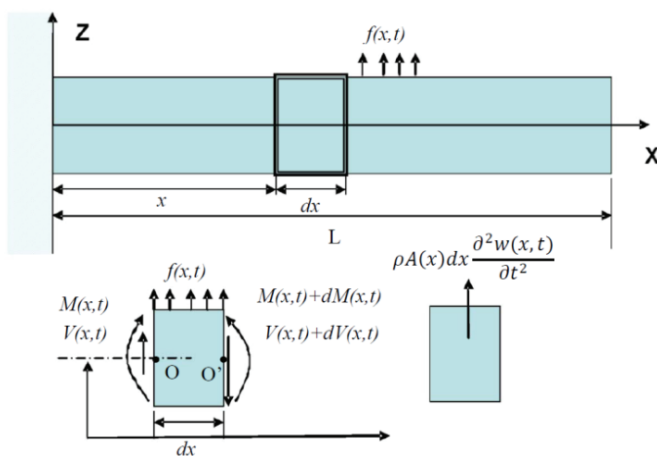$V(x,t)$ $V(x,t)+dV(x,t)$

O O

dx

Figure 4: Free body diagram of a beam in natural frequency analysis.

where $M(x,t)$ is the bending moment, $V(x,t)$ is the shear force, and $f(x,t)$ is the external force per unit length of the beam. Since the inertia force acting on the element of the beam is $\rho\, A(x)dx\frac{\partial^2 w(x,t)}{\partial t^2}$ the force equation of motion in the z direction gives

$$-(V+dV)+f(x,t)\,dx+V = \rho\, A(x)dx\frac{\partial^2 w(x,t)}{\partial t^2} \tag{4}$$

where ρ is the mass density and $A(x)$ is the cross-sectional area of the beam. The moment equation of motion about the y axis passing through point O in Fig. 4 leads to

$$(M+dM)-(V+dV)\,dx+f(x,t)\,dx\frac{dx}{2}-M=0 \tag{5}$$

By writing $dV=\frac{\partial V}{\partial x}dx$ and $dM=\frac{\partial M}{\partial x}dx$ and disregarding terms involving second powers in dx. The natural frequencies of the beam are computed from Eq. (6) as

$$\omega = \beta^2\sqrt{\frac{EI}{\rho A}} = (\beta l)^2\sqrt{\frac{EI}{\rho A l^4}} \tag{6}$$

where l is the length of the model, and ω is called the natural frequency of vibration. For any beam, there will be an infinite number of normal modes with one natural frequency associated with each normal mode. The cantilever beam with a fixed side and a free side could derive the Young's modulus and frequencies from Eq. (6) to Eq. (7)

$$E = \frac{4\pi^2 f_n^2 l^2 \rho A}{\lambda_n^4 I} \tag{7}$$

The density is equal to $(N_{atom}M_{element}/V_{total})$, where N_{atom} is the number of atoms, $M_{element}$ is the mass of the atom, V_{total} is the volume of the model, and f_n represents each resonant frequency of the atomic structure. In addition, λ_n is the constant of each resonant frequency (λ_1= 1.87 for the first mode, λ_2= 4.69 for the second mode, and λ_3= 7.85 for the third mode). I is the moment of inertia in the cross-sectional area. The ACM method has extensive applications; it can be applied in other nanostructured materials when the interatomic potential and the atomic structure of the material are known.

2.2 *Potential Function*

For the material properties of the spring element in the CNT structure, the Brenner's second-generation reactive empirical bond order (REBO) potential function [Brenner, Shenderova, Harrison, Stuart, Ni, and Sinnott (2002)] was broadly selected

to define the binding energy between carbon atoms, including the bond strength and the bond angle. The REBO defines the interatomic potential for carbon atoms as follows. The chemical binding energy E_b can be simply written as a sum over nearest neighbors in the form

$$E_b = \int_i \int_{j(>i)} \left[V^R(r_{ij}) - b_{ij} V^A(r_{ij}) \right] \tag{8}$$

where r_{ij} is the distance between atoms i and j, V^R and V^A are the repulsive and attractive pair terms, respectively. b_{ij} is a bond order between atoms i and j that is derivable from Huckel or similar level electronic structure theory.

The first-generation hydrocarbon expression used Morse-type terms for the pair interaction in Eq.(8). However, it was determined that this form is too restrictive to simultaneously fit equilibrium distances, energies, and force constants for carbon-carbon bonds. This form has the further disadvantage that both terms go to finite values as the distance between atom decreases, limiting the possibility of modeling processes involving energetic atomic collisions. In the REBO, the repulsive was shown in Eq. (9). And the attractive terms was shown in Eq. (10).

$$V^R(r) = f^c(r)(1 + Q/r)Ae^{-\alpha r} \tag{9}$$

$$V^A(r) = f^c(r) \int_{n=1,3} B_n e^{-\beta_n r} \tag{10}$$

The subscript n refers to the sum in Eq. (10), and r is the scalar distance between di-atoms. The screened Coulomb function used for the repulsive pair interaction (Eq. (9)) goes to infinity as interatomic distances approach zero, and the attractive term (Eq. (10)) has sufficient flexibility to simultaneously fit the bond properties that could not be fitted with the Morse-type terms used previously. The function $f^c(r)$ limits the range of the covalent interactions. The parameter fitting for carbon discussed below assumes a value of one for $f^c(r)$ for nearest neighbors and zero for all other interatomic distances. The general Abell-Tersoff form Eq. (8) is used for the total potential energy. Following the earlier hydrocarbon bonding expression, the empirical bond order function used here is written as sum of terms:

$$\bar{b}_{ij} = \frac{1}{2} \left[b_{ij}^{\sigma-\pi} + b_{ji}^{\sigma-\pi} \right] + b_{ij}^{\pi} \tag{11}$$

Values for the functions $b_{ij}^{\sigma-\pi}$ and $b_{ji}^{\sigma-\pi}$ depend on the local coordination and bond angles for atoms i and j, respectively. The function b_{ij}^{π} is further written as a sum of two terms:

$$b_{ij}^{\pi} = \pi_{ij}^{RC} + b_{ij}^{DH} \tag{12}$$

The value of the first term π_{ij}^{RC} depends on whether a bond between atoms i and j has radical character and is part of a conjugated system. The value of the second term b_{ij}^{DH} depends on the dihedral angle for carbon-carbon double bonds. Following the earlier hydrocarbon effort, the first term in Eq. (11) is given as

$$b_{ij}^{\sigma-\pi} = \left[1 + \int_{k(\neq i,j)} f_{ik}^c(r_{ik}) G\left(\cos(\theta_{ijk})\right) e^{\lambda_{ijk}} + P_{ij}\left(N_i^C, N_i^H\right) \right]^{-1/2} \tag{13}$$

The function $f^c(r)$ ensures that the interactions include nearest neighbor only. The function P represents a bicubic spline and the quantities N_i^C and N_i^H represent the number of carbon and hydrogen atoms, respectively, that are neighbor of atom i. The term π_{ij}^{RC} in Eq. (11) represents the influence of radical energetics and π-bond conjugation on the bond energies. As discussed in relation to the first-generation form of this potential, this term is necessary to correctly describe radical structures such as the vacancy formation energy in diamond, and to account for non-local conjugation effects such as those that govern the different properties of the carbon-carbon bonds in graphite and benzene. This function is taken as a tricubic spline F:

$$\pi_{ij}^{RC} = F_{ij}\left(N_i^t, N_j^t, N_{ij}^{conj}\right) \tag{14}$$

That depends on the total number of neighbors of bonded atoms i and j. And N_{ij}^{conj} depends on local conjugation. The term b_{ij}^{DH} in Eq. (12) is given by

$$b_{ij}^{DH} = T_{ij}\left(N_i^t, N_j^t, N_{ij}^{conj}\right) \left[\int_{k(\neq i,j)} \int_{l(\neq i,j)} \left(1 - \cos^2\left(\Theta_{ijkl}\right)\right) f_{ik}^c(r_{ik}) f_{jl}^c(r_{jl}) \right] \tag{15}$$

The value of $f^c(r)$ is defined by a cut-off radius function of the form

$$f_{ij}^c = \begin{cases} 1 & r < D_{ij}^{min} \\ \left[1 + \cos\left(\left(r - D_{ij}^{min}\right) / \left(D_{ij}^{max} - D_{ij}^{min}\right)\right)\right]/2 & D_{ij}^{min} < r < D_{ij}^{max} \\ 0 & r > D_{ij}^{min} \end{cases} \tag{16}$$

where $D_{ij}^{max} - D_{ij}^{min}$ defines the distance over which the function from one to zero. The problem comes in defining the nearest-neighbor distance. In diamond the nearest-neighbor distance is 1.54 Å, and in graphite the second-neighbor distance is 2.46 Å. To describe both structures, the function must go from one to zero between 1.54 and 2.46 Å. Because this is a rather abrupt cut-off, it is advantageous to maximize the difference between D^{max} and D^{min}.

All inter-atomic forces described using the empirical potential function can be transferred into the atomic force with springs to construct the atomic structure. This study implemented the commercial software ANSYS$^{®}$ to demonstrate the finite-element modeling and simulations. The ACM model for the CNT was based on the accuracy of the potential energy. The tensile and modal analyses both had the Young's modulus of approximately 1 TPa, which fell within the range of the Young's modulus in reported literature [Conwell and Wille (1997); Chang and Gao (2003)].

2.3 CNTs

A CNT is a hollow structure formed by sheets of graphene. The chiral vector describes the sheets rolled at specific directions, the radius, and the arrangement of hexagonal cells in the nanotube, as shown in Fig. 5. The chiral type depends on the θ (the angle between $\mathbf{a_1}$ and $\mathbf{a_2}$) and armchair type ($\theta = 0°$) and zigzag type ($\theta = 30°$) are generally chiral types. The chiral vector (C_h) is defined by the unit vector ($\mathbf{a_1}$, $\mathbf{a_2}$) and the graphene sheet lattice translation indices (n_1, n_2): $C_h = n_1 \overrightarrow{\mathbf{a}}_1 + n_2 \overrightarrow{\mathbf{a}}_2$, where n_1 and n_2 are integers. The relative parameters were as follows: carbon-carbon distance: $a_{c-c} = 1.44$ Å; unit vector $\overrightarrow{\mathbf{a}}_1 = \left(\sqrt{3}/2, \ 1/2\right) a$, $\overrightarrow{\mathbf{a}}_2 = \left(\sqrt{3}/2, \ -1/2\right) a$; length of chiral vector $L = |C_h| = a\sqrt{n_1^2 + n_2^2 + n_1 n_2}$ and diameter of CNT: $d_t = L/\pi$. The multi-walled nanotubes were considered as an assembly of multiple concentric SWNTs with a layer spacing of about 0.34 nm. In continuum mechanical analysis, the elastic modulus can be obtained not only
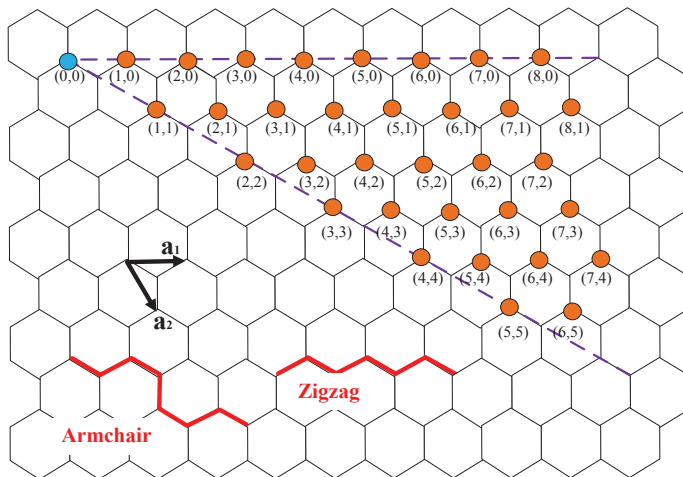

Figure 5: Graphitic sheet showing the basis vectors $\mathbf{a_1}$ and $\mathbf{a_2}$ of the two-dimensional unit cell.

through traditional tensile experiment, but also through modal analysis. Several case studies [Chiang, Chou, Wu, Huang, and Yew (2008); Chiang, Chou, Wu, and Yuan (2006); Wu, Chou, Han, and Chiang (2009)] are presented in the reference to validate the ACM method. In addition, the ACM could obtain the Young's modulus with high efficiency through tensile and modal analyses of the same model. ACM has higher efficiency than MD and MC, among others.

3 Modeling and Analysis

3.1 *ACM modeling and results*

The carbon-hydrogen bond energy can be derived by the bond-additive energies for molecular carbon-carbon single, double, conjugated double and triple bonds. The final parameter values were adopted to derive the carbon atomic potential Eq. (8) as shown in Tab. 1 and Tab. 2. The function $G_C\left(\cos\left(\theta_{ijk}\right)\right)$ in Eq. (13) modulates the contribution that each nearest neighbor makes to the empirical bond order according to the cosine of the angle of the bonds between atoms i and k and atoms i and j. The parameters were shown in Tab. 3.

Table 1: Parameters for the carbon-carbon pair term [Brenner, Shenderova, Harrison, Stuart, Ni, and Sinnott (2002)]

$B_1 = 12388.79\ eV$	$\beta_1 = 4.720452\ \overset{\circ}{A}^{-1}$	$Q = 0.31346029608\ \overset{\circ}{A}$
$B_2 = 17.56740\ eV$	$\beta_2 = 1.433213\ \overset{\circ}{A}^{-1}$	$A = 10953.544162\ eV$
$B_3 = 30.71493\ eV$	$\beta_3 = 1.382691\ \overset{\circ}{A}^{-1}$	$\alpha = 4.736539060\ \overset{\circ}{A}^{-1}$
$D_{min} = 1.7$	$D_{max} = 2.0$	

Table 2: Parameters for the b_{ij} to the carbon bond order [Brenner, Shenderova, Harrison, Stuart, Ni, and Sinnott (2002)]

	λ_{ijk}	$P_{ij} = 0$	$f^c(r)$	π_{ij}^{RC}	$\theta_{ijk} = 120^0$
value	0	0	1	-0.30113	$G\left(\theta_{ijk}\right) = 0.0528$

The force-displacement material properties of CNTs could be determined by Eqs. (17) and (18), which was derived using the differentiating Eqs. (9) and (10) with respect to displacement

$$\frac{\partial V^R(r)}{\partial r} = f^c(r)A\left[-\alpha e^{-\alpha r} - Qr^{-2}e^{-\alpha r} - \alpha Qr^{-1}e^{-\alpha r}\right] \tag{17}$$

$$\frac{\partial V^A(r)}{\partial r} = f^c(r) \int_{n=1,3} -\beta_n B_n e^{-\beta_n r} \tag{18}$$

Table 3: Parameters for the angular contribution to the carbon bond order [Brenner, Shenderova, Harrison, Stuart, Ni and Sinnott (2002)]

θ (rad)	G(cos(θ))	dG/d(cos(θ))	d^{2}G/d(cos(θ))^2	$\gamma(\theta)$
0	8	–	–	1
$\pi/3$	2.0014	–	–	0.416335
$\pi/2$	0.37545	–	–	0.271856
0.6082π	0.09733	0.400	1.980	–
$2\pi/3$	0.05280	0.170	0.370	–
π	-0.001	0.104	0.000	–

The CNT force-elongation of the two-body term can be illustrated by Fig. 6 (a). On the other hand, the relationship between force and angle of the three-body term is shown in Fig. 6 (b).

(a)

(b)
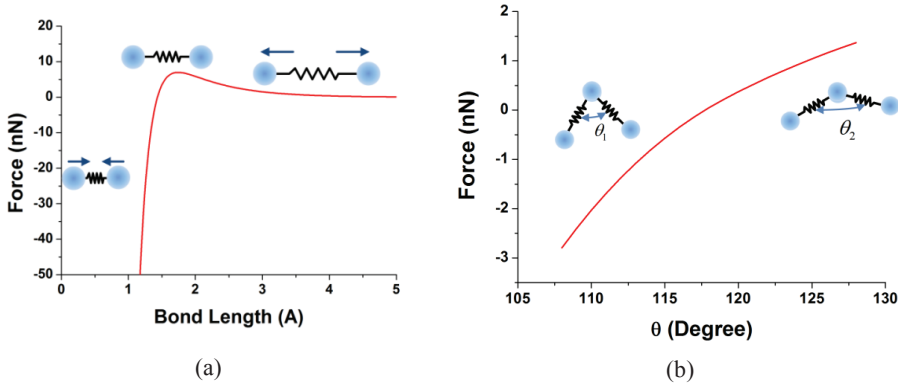
Figure 6: The relationship between (a) force and bond elongation; (b) force and bond angle.

The atomic structure of a CNT is constructed by atomic and bonding distributions. The atomic distribution of the hexagonal pattern was arranged using the methodology of [Dresselhaus, Dresselhaus, and Saito (1995)] which provided the modeling process. In the CNT modeling, covalent bonds are the main chemical bonds between each carbon atoms with characteristic bond length, bond angle, and dihedral

angle building up a hexagonal structure on the cylindrical wall of the nanotube. The processes of ACM modeling are shown in Fig. 7, which is described as follows:

1. The bonding force (interaction force between diatoms) is described by artificial spring element (force-elongation curve from REBO) as shown in Fig. 7 (a).

2. There is a two-body bonding term in the hexagonal structure, as described in Fig. 7 (b).

3. Fig. 7 (c) shows corner of the hexagonal structure deformation condition, where the solid black line shows the undeformed condition and the dashed blue line shows the small deformed condition. The geometry assumptions can derive the relationship Eq. (19) and (20).

$$\frac{\triangle l}{2} = R_{c-c}\frac{\triangle \theta}{2}, \quad \triangle \theta = \frac{\triangle l}{R_{c-c}} \quad . \tag{19}$$

$$\frac{1}{2}K_\theta \triangle \theta^2 = \frac{1}{2}k_{\theta'}\triangle l^2, \quad k_{\theta'} = K_\theta \frac{\triangle \theta^2}{\triangle l^2} = \frac{K_\theta}{R_{c-c}^2}. \tag{20}$$

The bond angle could equivalent into bond stretch using Eq.(20).

4. The three-body terms (dashed red line) of the hexagonal structure are illustrated in Fig. 7 (d).

5. ANSYS® software was utilized to derive the mechanical properties of the CNTs with tensile and modal analyses. The whole SWNT structure is shown in Fig. 7 (e).

As boundary conditions for Young's modulus analysis, one end of the ACM model is fully fixed, and the other end is applied constant small strain along axial direction in the tensile analysis. Beside, ACM model could also use only half of the model, together with symmetrical boundary conditions. This was done to reduce the CPU time during the simulation. Fig. 8 (a) shows a small displacement, which is 0.1% of the total length, along the axial direction of the SWNT. Fig. 8 (b) presents the boundary condition for modal analysis; it fixes all DOF on one side without any external loading.

The ACM model with tensile loading assumes that the stresses acting on each section are uniformly distributed, as shown in Fig. 8 (c). In the modal analysis, each atom considered includes the mass of the carbon nucleus and neglects the mass of the electrons. Meanwhile, by considering the atomic structure of carbon atom, the
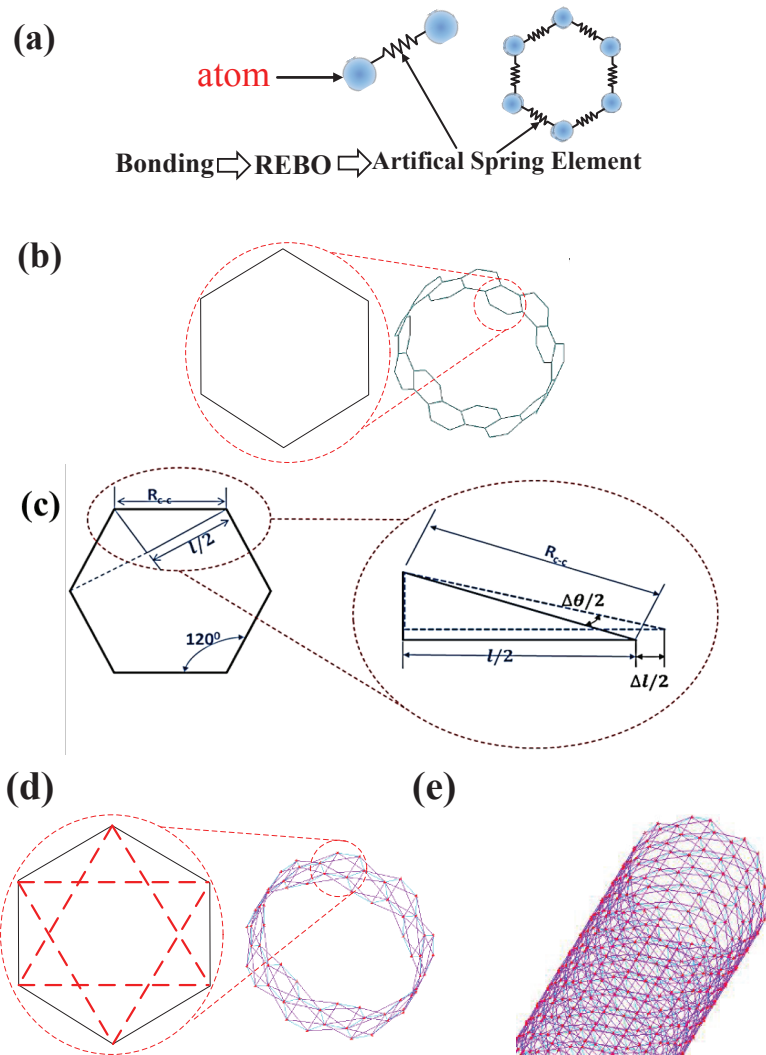
Figure 7: ACM modeling process: (a) All interatomic bonding forces (diatom and hexagonal structures) transforming to atomic force with springs to form the ACM model by REBO. (b) The hexagonal structure of the CNT contains a two-body term (solid black line), and (c) each corner is assumed to have a small deformation. (d) The hexagonal structure of the CNT contains two-body term (solid black line) and a three-body term (dashed red line). (e) Part of the SWNT structure.

mass of carbon nucleus ($m_{carbon} = 1.99 \times 10^{-23}$g), neglecting the mass of electrons, is assumed to be concentrated at the center of atom which is equivalent to the mass of node in the ACM model. The first three mode shapes are shown in Fig. 8 (d-1) to (d-3).
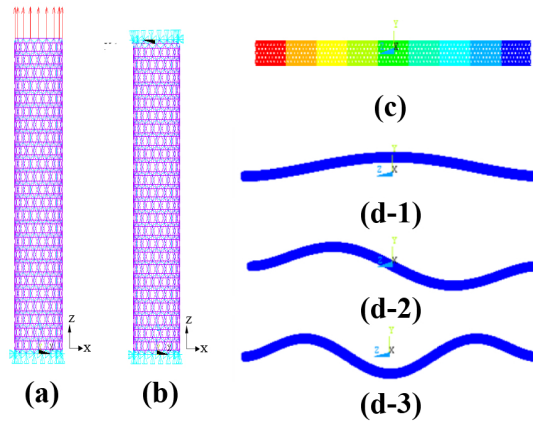
Figure 8: Boundary conditions for (a) tensile analysis and (b) modal analysis; (c) displacement distribution when the model is under tensile loading. Mode results: (d-1) first mode; (d-2) second mode; (d-3) third mode.

If the nanotubes are considered as continuum hollow beam, the cross-section area definition could be defined as shown in Eq. (21)

$$A = \pi dt \tag{21}$$

where d is the tude diameter, and t is the thickness. The thickness is taken as 0.34 nm the interlayer spacing of CNT [Dresselhaus, Dresselhaus, and Saito (1995)]. The moment of inertia is

$$I = \frac{\pi}{4}\left(r_o^2 - r_i^2\right) \tag{22}$$

where r_i and r_o are inner and outer radius of nanotubes. Therefore, the Young's modulus could be derived using the tensile and modal analysis. The Young's modulus of SWNTs can be derived using tensile loading method (Eq. (3)) and modal analyses (Eq.(7)) as shown in Tab. 4 and Fig. 9.

The Young's modulus of both tensile analysis and modal analysis is about 1,000 GPa, which falls within the range of the Young's modulus reported by [Conwell

Table 4: The Young's modulus of SWNTs at different chiral vector using tensile and modal analyses

	Chiral vector	(8,8)	(15,15)	(14,0)	(26,0)
	Length [nm]	80	80	80	80
	Elongation [%]	0.001	0.001	0.001	0.001
	Area [nm^2]	1.16	2.17	1.17	2.17
Tensile Analysis	Reaction force [pN]	0.012	0.022	0.012	0.023
	E (tensile) [GPa]	1,021	1,025	1,068	1,070
Modal Analysis	1st mode [Hz]	4.70E+09	8.84E+09	4.72E+09	8.76E+09
	2nd mode [Hz]	1.29E+10	2.40E+10	1.30E+10	2.38E+10
	3rd mode [Hz]	2.52E+10	4.69E+10	2.53E+10	4.61E+10
	E (1st mode) [GPa]	9.79E+02	1.05E+03	9.71E+02	1.03E+03
	E (2nd mode) [GPa]	9.81E+02	1.03E+03	9.73E+02	1.01E+03
	E (3rd mode) [GPa]	9.71E+02	1.02E+03	9.63E+02	9.88E+02

and Wille (1997)] (MD), [Salvetat, Briggs, Bonard, Bacsa, Kulik, Stöckli, Burnham, and Forró (1999); Yu, Files, Arepalli, and Ruoff (2000)](experimental result), and [Chang and Gao (2003)] (continuum theory). The ACM was based on the di-atom structure method which can exclude variety assumptions from microcosmic to macroscopic conditions. In the literature experimental result, the Young's modulus of CNT decreased from microcosmic to macroscopic. That indicated the CNT application and assumption influence proportional with the Young's modulus, such as the cross-sectional area definition.

3.2   CNT ropes

3.2.1   The categories of SWNTs cross-sectional area definition

The structure properties of CNT ropes utilized in the nanocomposite structure are in the main category of the CNT application. However, the structure property of CNT ropes (CNT bundles) has not been defined specifically until now. Therefore, there have been a number of cross-sectional area assumptions utilized in the literature. The four major types of cross-sectional area can be classified in Tab. 5. The cross-sectional area definitions include curve fitting by SEM [Yu, Files, Arepalli, and Ruoff (2000)], circumference multiplied by thickness [Pop, Mann, Wang, Goodson, and Dai (2006)], diameter [Zhang, Ichihashi, Landree, Nihey, and Iijima (1999)], and area of specific location [Salvetat, Briggs, Bonard, Bacsa, Kulik, Stöckli, Burnham, and Forró (1999)].
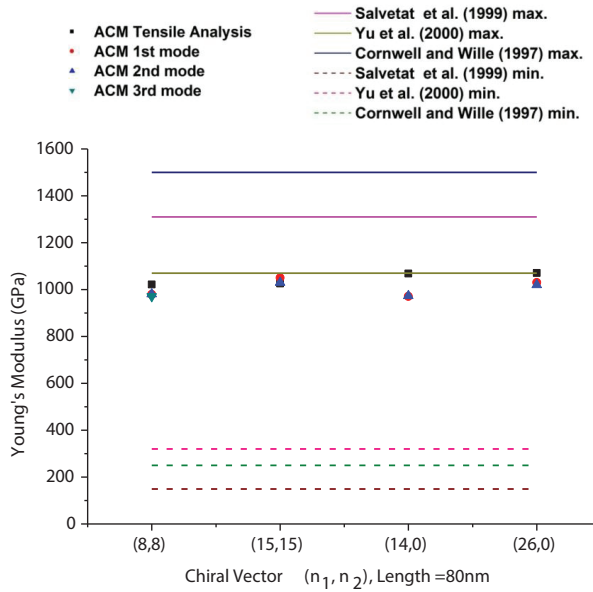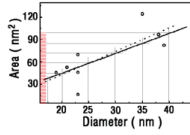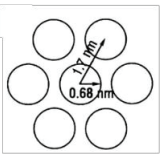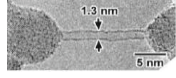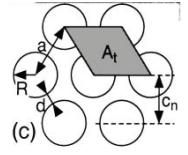
Figure 9: Young's modulus of SWNT estimation simulation results using tensile loading method and first three modes.

Table 5: CNTs with different cross-sectional area definitions

Figure				
Area Curve	fitting by $a(x-b)$	circumference πDt	diameter D	specific location $a^2 cos\pi/6$

3.2.2 *Cross-sectional area assumptions*

This study discussed two typical cross-sectional area types, including solid cross-sectional area and hollow cross-sectional area. The CNT structure was rolled from the grapheme sheets into a hollow tube. The inner diameter of each CNT was assumed to be too small to accommodate other elements. The CNT was arbitrary embedded into the material to transfer the external force; the force path involved grapheme occupation and inner diameter. Therefore, the CNTs resisted the external loading not only in the grapheme occupation but also in the inner diameter. In this

study, the distribution of CNT ropes were assumed to be in close-packed array. Three cross-sectional area assumptions were also used, as shown in Fig. 10. In the first case, the ropes of CNT were composited using the individual hollow circle, and the CNT ropes of the cross-sectional area were assumed to be equal to $2n\pi rt$, where n is the number of CNT, r is the radius of each CNT, and t refers to the wall-thickness of CNT. In the second case, the cross-sectional area of individual CNT was solid; thus, the solid area of the CNT ropes was equal to $n\pi r^2$. In the final case, the diameter of the ropes was equal to the maximum radius (R), and the cross-sectional area was equal to πR^2.
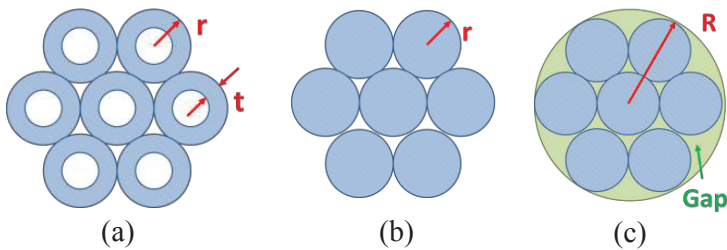
Figure 10: Cross-sectional area definitions of CNT rope: (a) individual hollow circle, (b) individual solid circle, and (c) total solid circumcircle.

The structure property of the CNTs was found to be independent of the diameter of the SWNTs when the cross-sectional area was defined by individual hollow or individual solid circles. The difference in the cross-sectional area definition between the individual hollow and individual solid circle was $2t/r$. When the chiral vector was (10, 10), the radius approached twice the well thickness; hence, the Young's modulus was very close regardless of whether the cross-sectional area was defined as hollow or solid. Furthermore, this study found a larger diameter of individual CNTs and a larger Young's modulus difference between individual hollow and solid areas. The results are shown in Table 6.

Table 6: Young's modulus difference between individual hollow and individual solid areas in different chiral vectors.

Chiral vector	Radius (nm)	E_{Hollow} (GPa)	E_{Solid} (GPa)
(10,10)	0.678	1037	1040
(12,12)	0.813	1037	867
(14,14)	0.949	1037	743
(16,16)	1.0848	1037	650

This study discusses the relationship between the Young's modulus and the three-kinds of cross-sectional area definitions, when the diameter of CNT clusters is distributed from 1.36 nm to 50 nm. The CNT clusters are composed using four kinds of chiral vectors of SWCNT, such as the chiral vector equal to (10,10) (diameter = 1.36 nm), (12,12) (diameter = 1.63 nm), (14,14) (diameter = 1.90 nm), and (16,16) (diameter = 2.17 nm). The Young's modulus distribution when the cross-sectional area of the CNT cluster is composed of an individual hollow circle is shown in Fig. 11 (a). The figure indicates that the Young's modulus will not decrease when the diameter of the CNT cluster increases. Clearly, the Young's modulus of the CNT cluster from the experimental result is dependent on the cross-sectional assumptions. Fig. 11 (b) shows the Young's modulus distribution when the cross-sectional area is composed of an individual solid circle. The difference between the individual hollow and the individual solid circle is *2t/r*. A larger diameter will lead to further differences between these two assumptions. Only the smaller diameter of the SWNT can decrease the difference for these two cross-sectional area assumptions. Fig. 11 (c) describes the Young's modulus distribution when the cross-sectional area is equal to a circumscribed circle. The circumscribed circle covers the SWNTs and the gaps among tubes.

The larger diameter of CNT cluster indicates the stable value of the ratio between the gap and the individual solid circles. That is the reason why the Young's modulus decreases when the diameter of CNT clusters increases. The circumscribed circle results also agree with the experimental results from the study of Sun and Chen (2009); Salvetat, Briggs, Bonard, Bacsa, Kulik, Stöckli, Burnham, and Forró (1999), which indicated a parabolic relationship between the tensile strength and the CNT diameter, as shown in Fig. 12 and Tab. 7. The Young's modulus of SWNTs approaches 400 GPa and has a similar trend when the cross-sectional area is assumed to be a circumscribed circle. Therefore, the circumscribed circle assumption might be closer to the cross-sectional area defined in the experimental operation.

Table 7: Young's modulus distribution in the different diameter and length [Gibson (2007)]

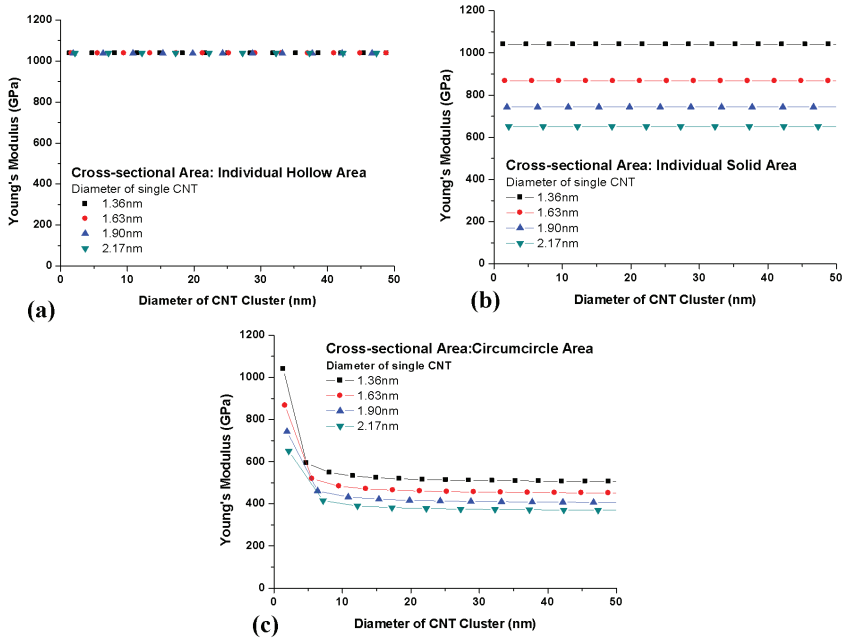| Material	Diameter (nm)	Length (nm)	Young's Modulus(GPa)
Vapor-grown	100-200	30,000-100,000	400-600
SWNT	˜1.3	500-40,000	320-1470

Figure 11: Young's modulus distribution when the cross-sectional area is defined as an (a) individual hollow circle, (b) individual solid circle, and (c) circumcircle.
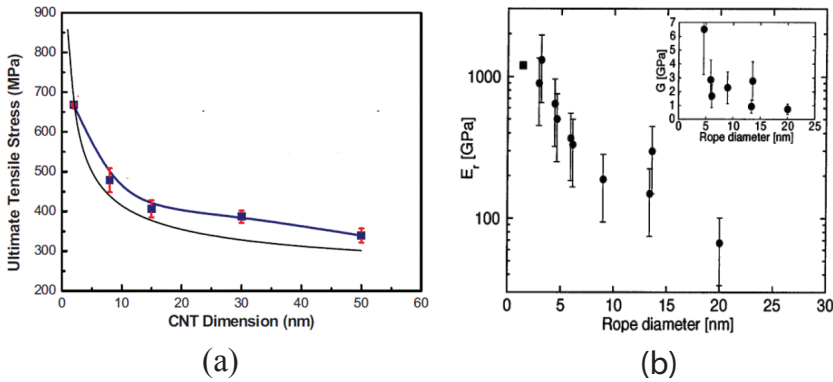

Figure 12: Relationship between the CNT diameter and the (a) ultimate tensile stress [Sun and Chen (2009)] and (b) reduced modulus [Salvetat, Briggs, Bonard, Bacsa, Kulik, Stöckli, Burnham, and Forró (1999)]

4   Equivalent Modeling

To date, simulations of the larger scale of the nanostructure are still limited, which raises the importance of using the equivalent method to reduce CPU time and obtain good agreement between the nanoscale and equivalent models. Papanikos, Nikolopoulos, and Tserpes (2008) proposed an atomistic-based FEM analysis, which is combined with the mechanics of materials to evaluate the geometrical characteristics and elastic properties of beams that have the same tensile, bending, and torsion behaviors as CNTs. Yuan and Chiang (2003) proposed a process that can be used to significantly reduce the CPU simulation time using an equivalent beam method based on the micro-macro technique.

The previous section result of the ACM method has been proven to be in agreement with the experimental result. As such, the following discussion is based on the mechanical behavior of the ACM. The adoption of a suitable element type to replace the ACM model is discussed at first. The goal of this section is to provide different equivalent element simulations that could remain the mechanical behavior. Thus, different models under the same tensile, vibration, shear, or torsion loading conditions should have similar mechanical behaviors. Therefore, the models are acceptable and have equivalent efficiencies. The individual CNT structure modeled by the ACM method is shown in Fig. 8. Exposure of the structure to different external loading conditions allows the rigidity of the structure to be obtained through its reaction force or displacement. Fig. 13 shows three types of boundary conditions of ACM model, including tensile, bending, and torsion.
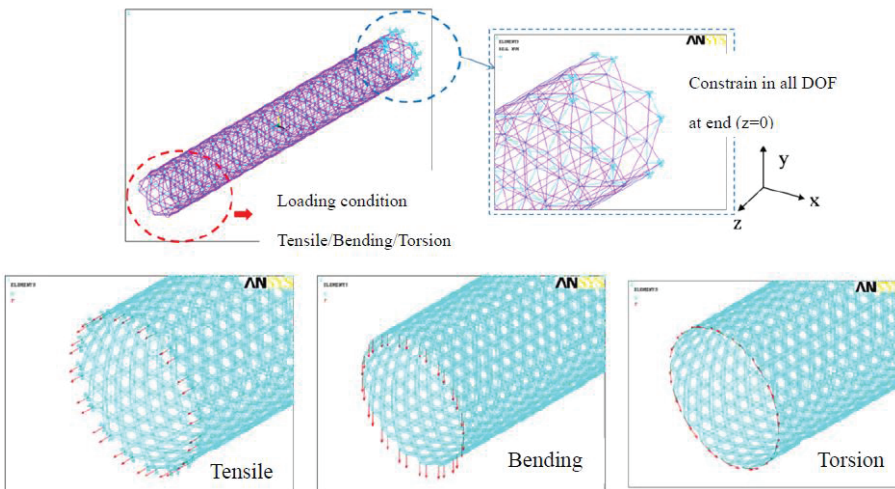

Figure 13: Equivalent boundary condition of the individual CNT.

The rigidity of the structure should be determined at first. To determine the relationship between displacement and loading condition, this study illustrates the three equations for each case. The tensile loading, bending, and torsion can be described by Eqs. (23), (24), and (25), respectively. In the tensile and bending conditions, the relationship between displacement and external loading are shown in Eqs. (23) and (24) as follows:
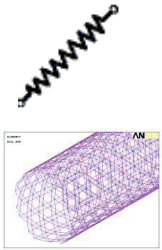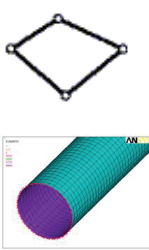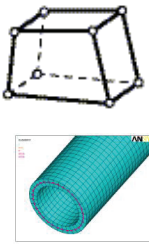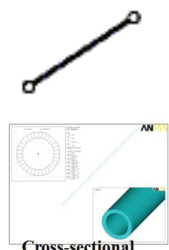
$$\delta_T = \frac{PL}{AE} \tag{23}$$

$$\delta_B = \frac{FL^3}{3EI} \tag{24}$$

$$\phi = \frac{TL}{GJ} \tag{25}$$

where δ is the deflection; P and F are the axial and bending forces, respectively; L is the length of the structure; E is the modulus of elasticity; A is the cross-sectional area; I is the moment of inertia; ϕ is the angle of twist; G is the shear modulus of elasticity; and J is the polar moment of inertia

Four kinds of element types are utilized in the present study to significantly reduce CPU simulation time. All of these four elements are briefly described below, and a summary is presented in Tab.8.

Table 8: Element properties of Combin39, Shell 181, Solid 45, and Beam 44.

Element Type	Combin39 (ACM method)	Shell181	Solid45	Beam44
Node/Space	2 node/ 3D space	4 node/ 3D space	8 node/ 3D space	2 node/ 3D space
DOF	6 DOF	6 DOF	3 DOF	6 DOF
Figure				
Application				Cross-sectional

(1) Combin39 is a unidirectional element with nonlinear generalized force-deflection capability that can be used in any analysis. This element has longitudinal or torsional capabilities in one-dimensional, two-dimensional, and three-dimensional applications. (2) Shell181 is suitable for analyzing thin to moderately-thick shell

structures, and has a four-node element with six DOFs at each node: translations in the x, y, and z directions, and rotations on the x, y, and z-axes. (3) Solid45 is used for three-dimensional modeling of solid structures. The element is defined by eight nodes that have three DOFs at each node, including translations in the nodal x, y, and z directions. (4) Beam44 is a uniaxial element with tension, compression, torsion, and bending capabilities that has six DOFs at each node, including translations in the nodal x, y, and z directions and rotations on the nodal x, y, and z-axes.

The equivalent of the CNT structure process is obtained through the following method. The chiral vector (15, 15) and length of SWNT is set at 100 nm. The three-dimensional, two-dimensional, and one-dimensional equivalent elements can be described using solid, shell, and beam elements, respectively. By comparing the analytical solution of the CNT structure with the simulation results of equivalent-continuum solid/shell/beam model, the reasonable wall-thickness of CNT, which is 0.34 nm in most studies, is acquired. The different equivalent models under the same tensile, vibration, shear, or torsion loading conditions would be discussed as follow:

4.1 Modal Analysis

The mode shapes of the equivalent models are shown in Fig. 14. All equivalent models illustrated the first mode is one-half sine wave, the second mode is one sine wave, and the third mode is one and half sine waves. The frequency distribution in the different equivalent model is shown in Fig. 15, which exhibit equivalent models and ACM model have the similar frequency distribution. That indicated the ACM model could be replaced by the equivalent model in the vibration condition.
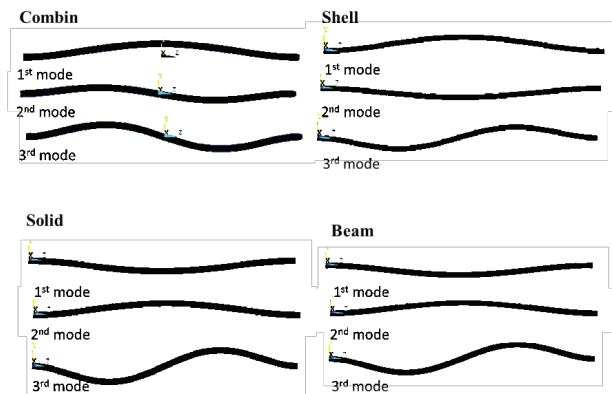

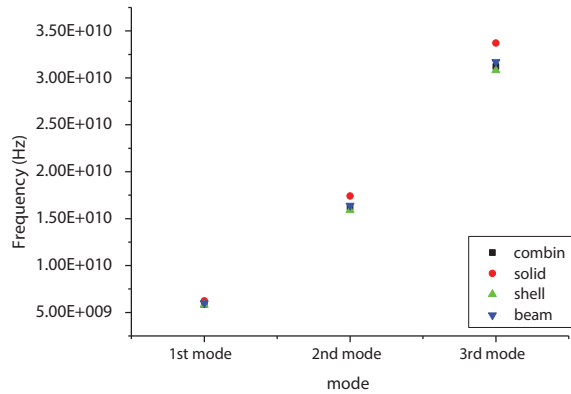Figure 14: The equivalent CNT model results in the modal analysis.

Figure 15: The equivalent CNT frequency distribution in the modal analysis.

4.2   Tensile Analysis

One end of the equivalent CNT models are applied the same external tensile loading (0.05 nN) in z direction, and the other end is fixed all DOFs. The displacement distributions of the equivalent models are shown in Fig. 16. All of them have the similar displacement distribution. In addition, Fig. 17 shows the maximum displacement distribution that indicated the displacement value difference are very small. That indicated the ACM model could be replaced by the equivalent model in the tensile condition.
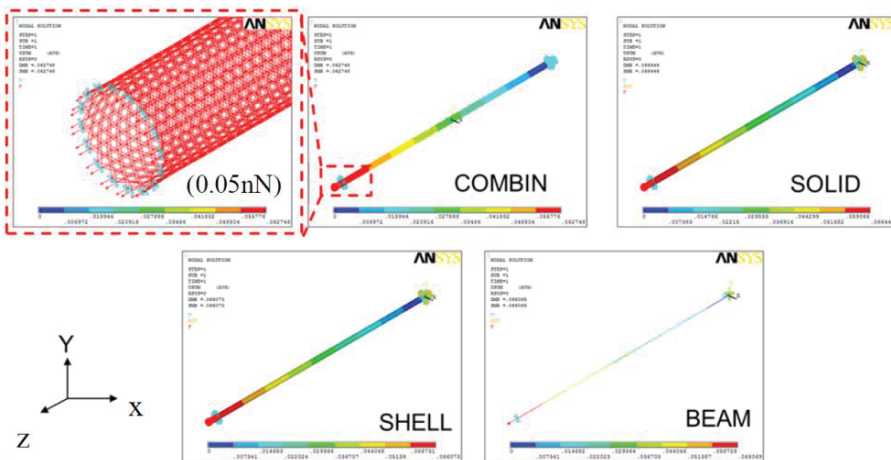

Figure 16: The equivalent CNT model results in the tensile analysis
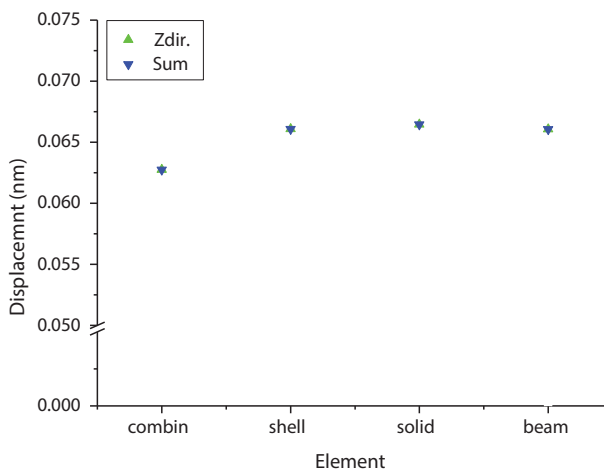
Figure 17: The equivalent CNT model displacement distribution in the tensile analysis

4.3 Bending Analysis

One end of the equivalent CNT models is applied the same external bending (0.5 pN) in y direction, and the other end is fully fixed. The displacement distributions of the equivalent models are shown in Fig. 18. All of them have the similar displacement distribution. In addition, Fig. 19 shows the maximum displacement distribution that indicated the difference of displacement values are very small. That result indicated the ACM model could be replaced by the equivalent model in the bending condition.

4.4 Torsion Analysis

One end of the equivalent CNT models is applied the torsion force (0.001 pN) in tangential direction, and the other end is fully fixed. The torsional angle distributions of the equivalent models are shown in Fig. 20. All of them have the similar displacement distribution. In addition, Fig. 21 shows the maximum torsion angle distribution that indicated the torsion angle value difference is very small. That indicated the ACM model could be replaced by the equivalent model in the torsion condition.

This section shows the displacement value and the differences in the Young's modulus among modes frequency, tensile, shear, and torsion analysis in Fig. 22 and Tab. 9. Fig. 22 illustrates the acceptability and trustworthiness of all these equivalent
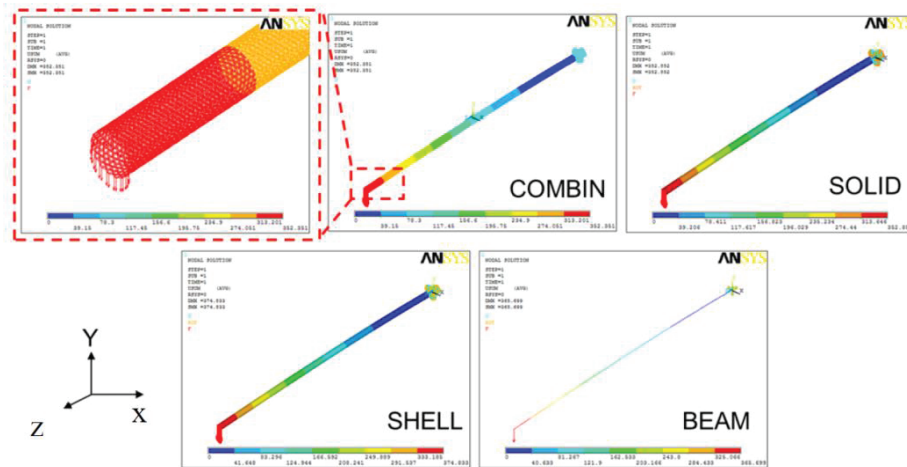
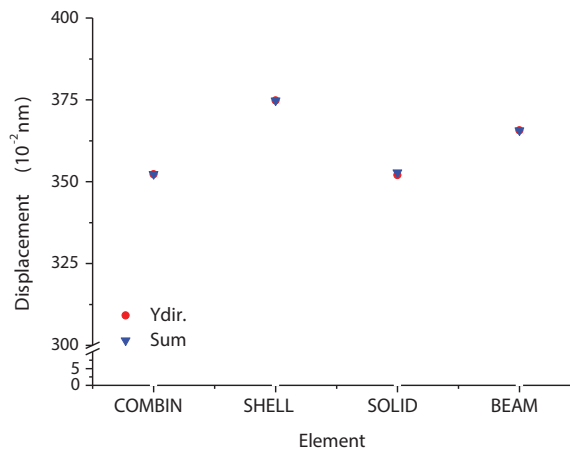Figure 18: The equivalent CNT model results in the bending analysis.

Figure 19: The equivalent CNT model displacement distribution in the bending analysis.

elements. The differences for all the analysis results are less than 6%. Adopting these equivalent models could contribute to maintaining the physical behavior of the displacement using different boundary conditions. The equivalent models are sufficiently accurate to present the mechanical behavior of CNT. The computer equipment used has the following properties: Intel Core 2, CPU 2.66 GHz, and
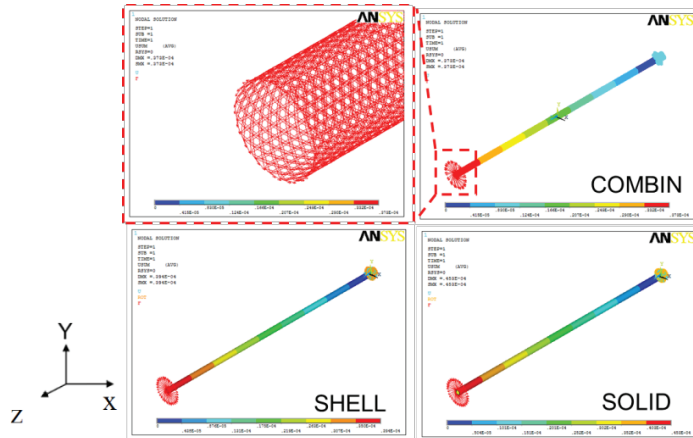
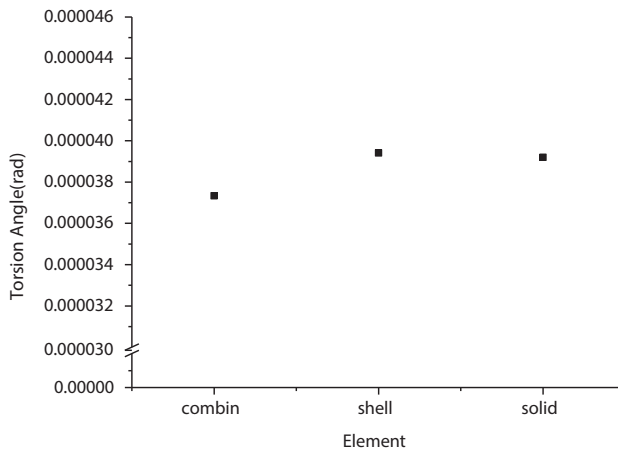Figure 20: The equivalent CNT model results in the torsion analysis.

Figure 21: The equivalent CNT model torsion angle distributions in the torsion analysis.

2.0 GB RAM. Fig. 23 presents the total element number and CPU time for each equivalent element. The CPU time depends on the total number of each equivalent model.
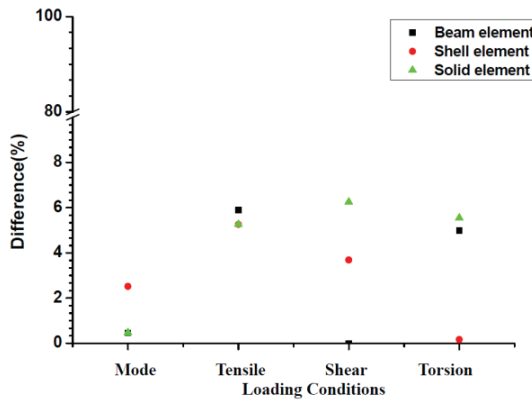
Figure 22: Difference in percentage among beam, shell, and solid elements based on the ACM model.
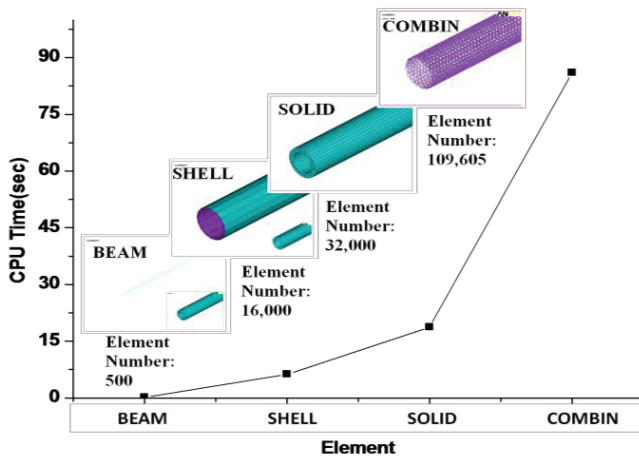
Figure 23: CPU time with different equivalent models.

Table 9: The CNT equivalent model results with different boundary conditions adopted Combin, Beam, Shell, and Solid elements.

	Tensile [nm]	Shear [nm]	Torsion [rad]
Combin	0.0627	3.52	0.373e-4
Shell	0.0660	3.74	0.394e-4
Solid	0.0664	3.52	0.383e-4
Beam	0.0660	3.65	N/A

5   Conclusions

The ACM transfers an originally discrete atomic structure into an equilibrium continuum model, and does not require the assumption of the Young's modulus and the cross-sectional area of each chemical bond. The ACM models based on FEM with equivalent-spring elements are proposed to investigate the Young's modulus and the modal analysis of nano-scale structures. All interatomic forces that are described using the empirical potential function can be transferred into atomic forces with springs to construct the atomic structure. The tensile and modal analysis results are in good agreement with the experiment results described in the literature. This study explored the ACM method to estimate the mechanical properties of an atomic-level structure through a proper potential energy. All results were validated using experimental results from literature. The ACM results are dependent on the following factors. First, the potential function is based on known properties. In relation to the properties of a new type of molecule, an appropriate force field may not be available for that type of molecule. Second, because ACM models are assembled by groups of springs, they cannot be used to predict the electronic properties of molecules. Moreover, this novel simulation method to investigate nano-scale materials is not limited to specific materials; it can be applied to any nano-structure materials once the inter-atomic potential and the atomic structure of the material are known. The ACM model can properly describe the mechanical properties of CNTs. From the CNT mechanical properties perspective, the CNT mechanical behavior could be presented using the ACM model based on the REBO potential function.

This study adopted three cross-sectional area assumptions to investigate the Young's modulus of CNT ropes. The first assumption indicates that the CNT ropes is composed by individual hollow CNT (the cross-sectional area of CNT rope $A_1 = 2n\pi rt$, where n is the number of CNT, r is the radius of each CNT, and t is the wall-thickness of CNT). The results showed that the Young's modulus does not depend on the diameter because the real CNT is a hollow tubular structure. The second cross-sectional area assumption comprised the individual solid CNT ($A_2 = n\pi r^2$). The difference between these two assumptions is a constant value ($A_1/A_2 = 2t/r$). Hence, the second assumption shows that the Young's modulus decreases when the diameter of individual CNT is larger. The third cross-sectional area assumption adopted the circumcircle area ($A_3 = \pi R^2$, where R is the radius of the CNT ropes). The circumcircle assumption contains the distribution of the tubes and the gaps between each tube. The ratio between the gaps and the tube areas becomes a stable value when the diameter of the CNT ropes is increased. Therefore, the larger the diameter of CNT ropes representing the Young's modulus, the more stable is the value, as proven by prior studies. The results indicate that the circumscribed circle

assumption might be a major option in the experimental operation in tensile and model testing.

This study investigated the equivalent solid, shell, and beam models to generate similar mechanical behaviors with the ACM model to reduce the CPU processing time. The equivalent models are accurate enough to be accepted, and can be used to obtain the mechanical behavior of CNTs through less element number. The equivalent methodology is based on the ACM method. This study investigates the equivalent solid/shell/beam model to reduce the CPU time by 60% to 80% and to maintain the accuracy of the ACM model. The equivalent solid/shell/beam models generate accurate ACM analysis results and significantly reduce the required CPU time. The equivalent models are accurate enough to be accepted and they can be used to obtain the Young's modulus of a greater number of CNTs.

Acknowledgement

References

Ávila, A. F.; Lacerda, G. S. R. (2008): Molecular mechanics applied to single walled carbon nanotubes. *Mat. Res.*, vol. 11, no. 3, pp. 325–333.

Brenner, D. W.; Shenderova, O. A.; Harrison, J. A.; Stuart, S. J.; Ni, B.; Sinnott, S. B. (2002): A second-generation reactive empirical bond order (REBO) potential energy expression for hydrocarbons. J. *Phys.: Condens. Matter*, vol. 14, no.4, pp. 783–802.

Chen, X.; Zhang, S.; Dikin, D. A.; Ding, W.; Ruoff, R. S.; Pan, L.; Nakayama, Y. (2003): Mechanics of a carbon nanocoil. *Nano Lett.*, vol. 3, no. 9, pp. 1299–1304.

Chang, T. C.; Gao, H. J. (2003): Size-dependent elastic properties of a single-walled carbon nanotube via a molecular mechanics model. *J. Mech. Phys. Solids*, vol. 51, no.6, pp. 1059–1074.

Chang, T. (2007): Torsional behavior of chiral single-walled carbon nanotubes is loading direction dependent. *Appl. Phys. Lett.*,vol. 90, pp. 201910–1–201910–3.

Cheng, H. C.; Hsu, Y. C.; Chen, W. H. (2009). The influence of structural defect on mechanical properties and fracture behaviors of carbon nanotubes. *CMC-Comput. Mat. Contin.*, vol. 11, no. 2, pp.127–146.

Chiang, K. N.; Chou, C. Y.; Wu, C. J.; Huang, C. J.; Yew, M. C. (2008): Analytical solution for estimation of temperature-dependent material properties of

metals using modified Morse potential. *CMES: Computer Modeling in Engineering & Sciences,* vol. 37, no. 1, pp.85–96.

Chiang, K. N.; Chou, C. Y.; Wu, C. J.; Yuan, C. A. (2006): Prediction of the bulk elastic constant of metals using atomic-level single-lattice analytical method. *Appl. Phys. Lett.*, vol. 88, pp.171904–1–171904–3.

Chung, J.W.; Hosson, J.Th.M. De; Giessen, E. van der (2002): Scaling of the failure stress of homophase and heterophase three-dimensional spring networks. *Phys. Rev. B*, vol. 65, pp. 094104–1–094104–8.

Conwell, C. F.; Wille, L. T. (1997): Elastic properties of single-walled carbon nanotubes in compression. *Solid State Commun.*, vol.101, no. 8, pp. 555–558.

Dresselhaus, M. S.; Dresselhaus, G.; Saito, R. (1995): Physics of carbon nanotubes. *Carbon*, vol.33, no. 7, pp.883–891.

Fan, C. W.; Liu, Y. Y.; Hwu, C. (2009): Finite element simulation for estimating the mechanical properties of multi-walled carbon nanotubes. *Appl. Phys. A-Mater. Sci. Process.*, vol. 95, no. 3, pp.819–831.

Gibson, R. F. (2007): Principles of composite material mechanics. second ed., CRC Press, New York.

Gusev, A. A. (2004): Finite Element Mapping for Spring Network Representations of the Mechanics of Solids. *Phys. Rev. Let.*, vol. 93, pp. 034302–1–034302–4.

Iijima, S. (1991): Helical microtubules of graphitic carbon. *Nature*, vol. 354, pp. 56–58.

Jalalahmadi, B.; Naghdabadi, R. (2006): Finite element modeling of single-walled carbon nanotubes with introducing a new wall thickness. *J. Phys.: Conf. Ser.*, vol. 61, pp. 497–502.

Jeng, Y. R.; Tsai, P. C.; Huang, G. Z.; Chang, I. L. (2009). An investigation into the mechanical behavior of single-walled carbon nanotubes under uniaxial tension using molecular statics and molecular dynamics simulations. *CMC-Comput. Mat. Contin.*, vol. 348, no. 1, pp.1–17.

Kis, A.; Cs?nyi, G.; Salvetat, J. P.; Lee, T. N.; Couteau, E.; Kulik, A. J.; Benoit, W.; Brugger, J.; Forr?, L. (2004): Reinforcement of single-walled carbon nanotube bundles by intertube bridging. *Nat. Mater.*, vol. 3, pp. 153–157.

Krishnan, A.; Dujardin, E.; Ebbesen, T. W.; Yianilos, P. N.; Treacy, M. M. J. (1998): Young's modulus of single-walled nanotubes. *Phys. Rev. B*, vol. 58, no. 20, pp. 14013–14019.

Lawrence, J. G.; Berhan, L. M.; Nadarajah, A. (2009): Elastic properties and morphology of individual carbon nanofibers. *ACS Nano.*, vol.2, no. 6, pp.1230–1236.

Liu, B.; Jiang, H.; Huang, Y.; Qu, S.; Yu, M. F.; Hwang, K. C. (2005): Atomic-scale finite element method in multi-scale computation with applications to carbon nanotubes. *Phys. Rev. B*, vol. 72, pp. 35435–1–35435–8.

Mote Jr., C. D. (1971): Global-local finite element. *Intl. J. Numer. Methods Eng.*, vol. 3, no. 4, pp.565–574.

Papanikos, P.; Nikolopoulos, D. D.; Tserpes, K. I. (2008): Equivalent beams for carbon nanotubes. *Comput. Mater. Sci.*, vol.43, no. 2, pp. 345–352.

Peng, R. D.; Zhou, H. W.; Wang, H. W.; Leon Mishnaevsky Jr., (2012): Modeling of nano-reinforced polymer composites: Microstructure effect on Young's modulus. *Comput. Mater. Sci.*, vol. 60, pp. 19–31.

Poncharal, P.; Wang, Z. L.; Ugarte, D.; de Heer, W. A. (1999): Electrostatic deflections and electromechanical resonances of carbon nanotubes. *Science*, vol. 283, no. 5407, pp.1513–1516.

Pop, E.; Mann, D.; Wang, Q.; Goodson, K.; Dai, H. (2006): Thermal conductance of an individual single-wall carbon nanotube above room temperature. *Nano Lett.*, vol. 6, no. 1, pp. 96–100.

Rao, S. S. (2005): Mechanical vibrations, fourth ed., Pearson/Prentice Hall, Singapore,.

Rossi, M.; Meo, M. (2009): On the estimation of mechanical properties of single-walled carbon nanotubes by using a molecular-mechanics based FE approach. *Compos. Sci. Technol.*, vol. 69, no. 9, pp. 1394–1398.

Ruoff, R. S.; Qian, D.;Liu, W. K. (2003): Mechanical properties of carbon nanotubes: theoretical predictions and experimental measurements. *C. R. Physique*, vol. 4, pp. 993–1008.

Salvetat, J. P.; Briggs, G. A. D.; Bonard, J. M.; Bacsa, R. R.; Kulik, A. J.; Stöckli, T.; Burnham, N. A.; Forró, L. (1999): Elastic and shear moduli of single-walled carbon nanotube ropes. *Phys. Rev. Lett.*, vol. 82, no. 5, pp. 944–947.

Sun, Y.; Chen, Q., (2009): Diameter dependent strength of carbon nanotube reinforced composite. *Appl. Phys. Lett.*, vol. 95, pp. 21901–1–21901–3.

Tserpesa, K. I.; Papanikos, P. (2009): Continuum modeling of carbon nanotube-based super-structures. *Compos. Struct.*, vol. 91, no. 2, pp. 131–137.

Voleti, S. R.; Chandra, N.; Miller, J. R. (1996): Global-local analysis of large-scale composite structures using finite element. *Comput. Struct.*, vol. 58, no. 3, pp. 453–464.

Wang, A. S. D.; Corssman, F. W. (1977): Some new results on edge effect in symmetric composite laminates. *J. Compos Mater.*, vol. 11, pp. 92–106.

Wu, C. J.; Chou, C. Y.; Han, C. N.; Chiang, K. N. (2009): Estimation and validation of elastic modulus of carbon nanotubes using nanoscale tensile and vibrational analysis. *CMES: Computer Modeling in Engineering & Sciences*, vol. 41, no. 1, pp. 49–67.

Yu, M. F.; Files, B. S.; Arepalli, S.; Ruoff, R. S. (2000): Tensile loading of ropes of single wall carbon nanotubes and their mechanical properties. *Phys. Rev. Lett.*, vol. 84, no. 24, pp. 5552–5555.

Yuan, C. A.; Chiang, K. N. (2003): Micro to macro thermo-mechanical simulation of wafer level packaging. *ASME trans. on Journal of Electronic Packaging*, vol. 125, pp. 576–581.

Zhang, Y.; Ichihashi, T.; Landree, E.; Nihey, F.; Iijima, S. (1999): Heterostructures of single-walled carbon nanotubes and carbide nanorods. *Science*, vol. 285, no. 5434, pp. 1719–1722.